View metadata, citation and similar papers at core.ac.uk

brought to you by CORE

provided by NASA Technical Reports Server

Simulated Time Lags of Hinode/XRT and SDO/AIA Lightcurves as an Indication of Loop Heating Scenario

C. E. Alexander[1], R. Lionello[2], A. R. Winebarger[1]

1 NASA Marshall Space Flight Center, Huntsville, AL 2 Predictive Science, Inc., 9990 Mesa Rim Road, Suite 170, San Diego, CA 92121-3933, USA

Contact email: caroline.e.alexander@nasa.gov

Abstract

The precise nature of the heating mechanism (location, duration) in coronal loops is still a matter of enormous research. We present results from a 1D hydrodynamic loop simulation of a coronal loop which was run using different parameters such as loops length (50, 200, and 500 Mm), maximum temperature reached (3MK and 10MK), and abundances. For each scenario the model outputs were used to calculate the corresponding lightcurves as seen by XRT/Be-thin and various EUV AIA channels. The lag time between the peak of these lightcurves was computed using cross-correlation and plotted as a function of loop length. Additional results were computed using the 0D EBTEL code in order to test the compatibility of the two codes and to investigate additional loop lengths. Initial results indicate that the long (>5000s) lags observed in the ~100Mm loops of active regions can only be reproduced using photospheric abundances and much longer loop lengths. This result suggests that the observed time lags cannot be completely explained by impulsive heating.

The heating and cooling of coronal loops

Finding the mechanism that is primarily responsible for heating the solar corona has been a continuous challenge to generations of solar physicists. Much is still not understood about the fundamental processes that create and maintain active region coronal loops, the brightest structures in the corona (Figure 1). We know that the free energy of the magnetic field is converted into heating, but we don't know how and where. An important and relatively easy measurement is the timescale for the evolution of coronal loops. The timing of the peaks and widths of the intensity evolution of coronal loops can be used to try and pin down the particulars of the heating. This is an important, ongoing debate as both the duration of the heating (impulsive vs steady) and the location of the heating along the loop have yet to be fully understood.

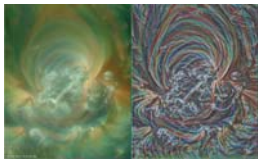

***Figure 1**: 3-color image of an active region showing data from SDO/AIA 193, 171, and 211 Å (left). The image on the right shows this data after being processed with a Gaussian filter and shows that individual loops are at different stages of cooling (i.e. show up in different wavelengths/colors).*

Lightcurves as a guide to heating scenario

EUV observations of coronal loops suggest what appears to be a general cooling trend, as their emission peaks first in channels associated with higher temperatures and later in those associated with lower (Winebarger et al. 2003; Ugarte-Urra et al. 2006; Mulu-Moore et al. 2011). Recently, Viall & Klimchuk (2012) described a technique to evaluate the temporal delays between different EUV channels on the Solar Dynamics Observatory's Atmospheric Imaging Assembly (SDO/AIA). Applying this technique onto AIA observations in different AIA channels, they produced a map of time lags and concluded that loops in the observed region are mostly cooling. In Viall & Klimchuk (2013), they endeavored to explain the observed lightcurves as the consequence of short nanoflare storms (Cargill et al. 1995; Cargill & Klimchuk 1997; Warren et al. 2002, 2003; Klimchuk 2006), in which the observationally unresolved strands composing a loop are impulsively heated at different times. Since the length of the storm, i.e. the interval between the first and last heating event is relatively short, the loop would then appear in channels associated with progressively lower temperatures as the plasma in the strands cools and drains down.

A great wealth of solar data is available to help investigate the properties of coronal loops. Instruments such as SDO/AIA and Hinode/XRT allow us to image the solar corona in numerous EUV and X-ray wavelengths. Figure 2 shows the temperature response curves of SDO/AIA along with the response of the Be-thin filter of XRT. This has been included for additional information hotter plasma.

The aim of this work is to determine whether the impulsive-heating paradigm can actually yield the observed time delays between peaks in different emission channels, and if not, to suggest a heating scenario that can.

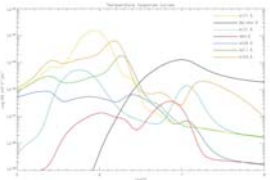

***Figure 2**: Temperature response curves of EUV and X-ray channels of SDO/AIA and Hinode/XRT*

Coronal Loop Model description

The model used in this analysis is the time-dependent, thermodynamic, hydrodynamic (HD) model of Mikic et al. (2013). We explore the parameter space of this model by computing the evolution of coronal loops with different lengths and element abundances that undergo impulsive heating, and are then left to cool. We consider semi-circular loops of three possible lengths: 50, 200, or 500 Mm, which correspond to meshes that have 732, 2928, and 7320 points respectively.

The minimum resolution in all loop models is 23 km at the footpoints, while the maximum resolution at the apex is 234 km. The expansion factor for each loop is shown in Figure 3a as a function of the length along the loop. At the footpoints of the loop we impose a fixed temperature (T = 20, 000 K) and electron density (n_e = 6×10^{12} cm^{-3}). Starting from arbitrary initial conditions, we specify a very small, constant, uniform heating $H_0 = 5 \times 10^{-9}$ erg cm^{-3} s^{-1}, and relax the system until we find the cold loop solutions, corresponding to the three loop lengths.

For each loop, having either coronal or photospheric abundances (Figure 4), we add to H_0 a triangular impulsive heating functions H_1(t), whose parameters are listed in Table 1. For each length, we consider a medium and a strong pulse, such that the apex temperature may reach 3 and 10 MK respectively (NB only the results from the 10 MK case are detailed here). In all cases, the pulses (base of the triangle) last for 500s.

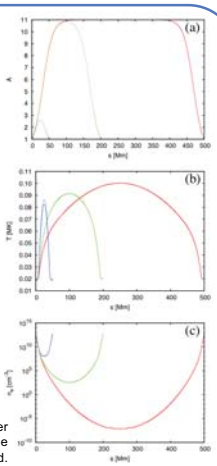

***Figure 3**: Area, temperature and density along the loop for 50, 200 and 500 Mm length (blue, green, red respectively.)*

Table 1. Impulsive Heating Parameters

Loop Length [Mm]	T_{max} [MK]	H_{max} [erg cm^{-3} s^{-1}]
50	3	3.5×10^{-2}
50	10	2.0×10^{-1}
200	3	1.2×10^{-2}
200	10	5.0×10^{-2}
500	3	5.3×10^{-3}
500	10	2.0×10^{-2}

Note. — We apply a triangular, uniform in space, heat pulse $H_1(t)$ during a 500 s interval. The first column shows the length of the loop to which the pulse is applied, the second the maximum temperature reached during the simulations in the case with coronal abundances, the third the maximum heating applied.

In order to explore the parameter space further, two versions of the radiative loss function were used. Figure 4 shows the two abundances (CHIANTI (v7.1) coronal and photo-spheric abundances*) compared to the two functions used by the EBTEL 0D code (Klimchuk et al. 2008) i.e. the RTV (red) and Raymond-Klimchuk (green) lines. EBTEL is used further in this study and some preliminary results are shown in the Future Work section.

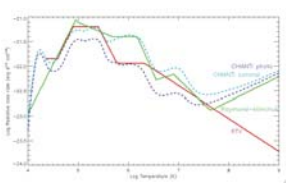

***Figure 4**: Comparison of the two radiative loss functions used in this study with the ones used by the EBTEL code. Our model used the CHIANTI coronal (blue dashed) and the CHIANTI photospheric abundances (purple dashed).*

* Abundances used were coronal (Feldman et al. 1992; Feldman 1992; Grevesse & Sauval 1998; Landi et al. 2002) and photospherei (Feld- man et al. 1992; Grevesse et al. 2007).

Investigating the model outputs

The outputs of the model are temperature and electron density and are shown in panel b and c of Figure 3. These outputs are used in conjunction with the SDO/AIA and Hinode/XRT response functions (see Figure 2) to compute the corresponding lightcurves. The time lags of the emission peaks in numerous EUV and X-ray channels can then be calculated using a cross-correlation technique. The relation between these time lags and the loop length can then be investigated.

Six variations of the parameter space were explored i.e. for coronal and photospheric abundances for each of the three different loop lengths. Figure 5 shows an example of one of the model runs. This example is for a 50 Mm loop using photospheric abundances. The top panel shows the evolution of the normalized temperature and density over time while the bottom panel shows the normalized lightcurves produced.

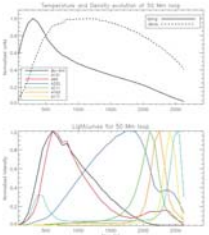

***Figure 5**: Example of the outputs of one of the six runs of the model. Top panel shows the temperature and density evolution over the duration of the simulation while the bottom panel shows the lightcurves SDO/AIA and XRT/ Be-thin would see if this were a real observation.*

This type of plot offers lots of useful information but the shape and width of the lightcurves is hard to explain. Figure 6 is used to help explain the pattern of the lightcurves. For each of the EUV/X-ray channels used, the temperature response function of that channel can be compared with the temperature evolution to explain the lightcurve in detail. The top panel of each plot shows the temperature over-plotted with the response curve. The response only relates to the y-axis (temperature) and not to the x-axis (time) to which it has been normalized against. The purpose of this is to indicate at what times the temperature falls within the sensitivity peaks of the response, thus, leading to a peak in the lightcurve. Any density changes in the loop can also severely affect the pattern of the lightcurves.

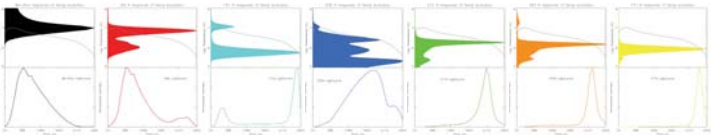

***Figure 6**: Investigation of the pattern of lightcurves for each of the seven passbands utilized. Each plot shows the relation between the temperature evolution of the loop during the simulation (grey line, top panel in each) and the temperature response function of each passband (filled color plot in each top panel). These response functions are normalized to the x-axis (as they have no relation to time) but are plotted on the same temperature axis (y-axis, top panels) as the temperature evolution. This allows us to see when the loop is at a temperature that each particular filter is sensitive to (i.e. its peaks). The bottom panel of each plot shows the resultant lightcurve. This approach makes it easy to explain the peak time of each lightcurve, as well as it's width (related to the amount of time spent at a temperature that filter is sensitive to), and other features such as double peaks. Results from the 94 and 131 Å channels have not been used for time lag analysis.*

Time lag analysis

The lightcurves produced give important clues about the heating of the loop plasma. In order to examine these intensity profiles further, the time between the peaks of various combinations of passbands are calculated. Table 2 gives details of the combinations used as well as the characteristic temperatures of the two filters in each comparison. The final column shows the difference between the two characteristic temperatures of the filters in each case. Larger differences in temperatures should lead to longer lag times for the plasma to cool through the passbands.

Wavelength comb.	Char. Temp 1	Char. Temp 2	Diff (MK)
Be-thin : 335 Å	10 MK	2.5 MK	7.5
Be-thin : 211 Å	10 MK	2 MK	8
Be-thin : 193 Å	10 MK	1.5 MK	8.5
Be-thin : 171 Å	10 MK	1 MK	9
335 Å : 211 Å	2.5 MK	2 MK	0.5
335 Å : 193 Å	2.5 MK	1.5 MK	1
335 Å : 171 Å	2.5 MK	1 MK	1.5
211 Å : 193 Å	2 MK	1.5 MK	0.5
211 Å : 171 Å	2 MK	1 MK	1
193 Å : 171 Å	1.5 MK	1 MK	0.5

***Table 2**: List of the combination of passbands used to measure time lags. 335 Å : 211 Å is greyed out as the results are not included in Figure 7. The characteristic temperatures of each passband is shown in the middle columns and the difference between the two is shown in the last column.*

Each of the wavelength combinations listed in Table 2 produces six values of time lag (one for each of the three loop lengths and two abundances used). These values can then be plotted on a graph of time lag vs loop length. Figure 7 shows the main results. The results using photospheric abundances are plotted in blue with coronal abundances in red.

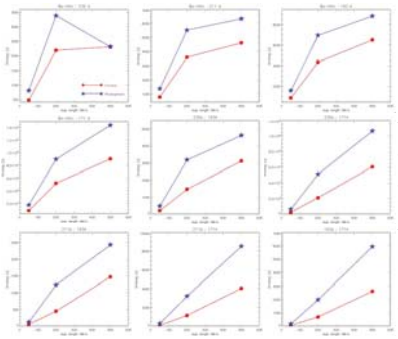

***Figure 7**: Results showing the time delays between the peaks of various pairs of passbands compared to loop length and abundance choice.*

The results show that:

- Longer loops taking longer to cool
- Time lags between passbands of similar temperatures are shorter than those further apart in temperature
- Loops using photospheric abundances take longer to cool than those using coronal abundances (due to the increase in density in these first loops).

These results are to be expected. The main outcome is that these plots indicate the length of time lags that should be expected if loops (of a particular length) are heated impulsively. Anything outside this would indicate another heating mechanism at work.

The results of Viall & Klimchuk (2012) focus on an active region where the typical loop length is <200Mm (based on measuring the field lines from a potential field extrapolation). They use an innovative method to plot the time lags measured from AIA data as 'time lag maps' to show which loops have the longest/shortest cooling time delay between the peaks in various passband combinations.

They investigate an active region over a 24 hour period and find that the majority of the AR loop structures are cooling. They measure time delays of up to 6000s for the various combinations – something that we are only able to achieve using much longer loop lengths and/or photospheric abundances. This disparity is something we intend to explore further before we can definitively comment on the applicability to impulsive heating models to coronal loop studies.

Conclusions and Future Work

We find evidence that impulsive heating may not tell the whole story about coronal loops. Our impulsively heated model cannot match the observed time lags calculated for a typical active region suggesting that another process, or combination of processes may be at work. Future work will expand upon this study by looking at other impulsive models such as EBTEL. Some initial results are shown in Figure 8 where it can be seen that the level of agreement between the codes can be hit or miss at this early stage.

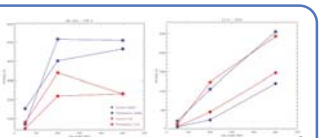

***Figure 8**: Example plots showing the same time lag analysis as above using our code and the EBTEL code for two different channel combinations. The left panel shows very different time lags for different loop lengths while the right panel shows good agreement.*

References

Cargill, P. J., & Klimchuk, J. A. 1997, ApJ, 478, 799

Cargill, P. J., Mariska, J. T., & Antiochos, S. K. 1995, ApJ, 439, 1034

Klimchuk, J. A. 2006, Sol. Phys., 234, 41

Klimchuk, J. A., Patsourakos, S., Cargill, P. 2008, ApJ, 682, 1351

Mikic, Z., Lionello, R., Mok, Y., Linker, J. A., & Winebarger, A. R. 2013, ApJ, 773, 94

Mulu-Moore, F. M., Winebarger, A. R., Warren, H. P., & Aschwanden, M. J. 2011, ApJ, 733, 59

Ugarte-Urra, I., Winebarger, A. R., & Warren, H. P. 2006, ApJ, 643, 1248

Viall, N. M., & Klimchuk, J. A. 2012, ApJ, 753, 35

Viall, N. M., & Klimchuk, J. A. 2013 ApJ, 771, 115

Warren, H. P., Winebarger, A. R., & Hamilton, P. S. 2002, ApJ, 579, L41

Winebarger, A. R., Warren, H. P., & Seaton, D. B. 2003, ApJ, 593, 1164